

**The impact of the spin–orbit misalignment and of the spin of B on the
Lense–Thirring orbital precessions of the Double Pulsar PSR
J0737–3039A/B**

Lorenzo Iorio¹

Ministero dell’Istruzione, dell’Università e della Ricerca (M.I.U.R.)
Viale Unità di Italia 68, I-70125, Bari (BA), Italy

lorenzo.iorio@libero.it

Received _____; accepted _____

Abstract

In the Double Pulsar, the Lense–Thirring periastron precession $\dot{\omega}^{\text{LT}}$ could be used to measure/constrain the moment of inertia \mathcal{I}_A of A. Conversely, if \mathcal{I}_A will be independently determined with sufficient accuracy by other means, tests of the Lense–Thirring effect could be performed. Such findings rely upon a formula for $\dot{\omega}^{\text{LT},A}$ induced by the spin angular momentum \mathbf{S}^A of A, valid if the orbital angular momentum \mathbf{L} and \mathbf{S}^A are aligned, and neglecting $\dot{\omega}^{\text{LT},B}$ because of the smallness of \mathbf{S}^B . The impact on $\dot{\omega}^{\text{LT},A}$ of the departures of the \mathbf{S}^A - \mathbf{L} geometry from the ideal alignment is calculated. With the current upper bound on the misalignment angle δ_A between them, the angles λ_A , η_A of \mathbf{S}^A are constrained within $85^\circ \lesssim \lambda_A \lesssim 92^\circ$, $266^\circ \lesssim \eta_A \lesssim 274^\circ$. In units of the first order post-Newtonian mass-dependent periastron precession $\dot{\omega}^{\text{GR}} = 16.89^\circ \text{ yr}^{-1}$, a range variation $\Delta\dot{\omega}^{\text{LT},A} \doteq \dot{\omega}_{\text{max}}^{\text{LT},A} - \dot{\omega}_{\text{min}}^{\text{LT},A} = 8 \times 10^{-8} \dot{\omega}^{\text{GR}}$ is implied. The experimental uncertainty $\sigma_{\dot{\omega}_{\text{obs}}}$ in measuring the periastron rate should become smaller by 2028-2030. Then, the spatial orientation of \mathbf{S}^B is constrained from the existing bounds on the misalignment angle δ_B , and $\dot{\omega}^{\text{LT},B} \simeq 2 \times 10^{-7} \dot{\omega}^{\text{GR}}$ is correspondingly calculated. The error $\sigma_{\dot{\omega}_{\text{obs}}}$ should become smaller around 2025. The Lense–Thirring inclination and node precessions \dot{I}^{LT} , $\dot{\Omega}^{\text{LT}}$ are predicted to be $\lesssim 0.05$ arcseconds per year, far below the current experimental accuracies $\sigma_{I_{\text{obs}}} = 0.5^\circ$, $\sigma_{\Omega_{\text{obs}}} = 2^\circ$ in measuring I , Ω over 1.5 year with the scintillation technique. The Lense–Thirring rate \dot{x}_A^{LT} of the projected semi-major axis x_A of PSR J0737–3039A is $\lesssim 2 \times 10^{-16} \text{ s s}^{-1}$, just two orders of magnitude smaller than a putative experimental uncertainty $\sigma_{x_A^{\text{obs}}} \simeq 10^{-14} \text{ s s}^{-1}$ guessed from 2006 data.

Keywords: gravitation – celestial mechanics – pulsars: general – pulsars: individual: PSR J0737–3039A– pulsars: individual: PSR J0737–3039B

1. Introduction

The double pulsar PSR J0737–3039A/B, discovered in 2003 (Burgay et al. 2003; Lyne et al. 2004), is a tight binary system made of two neutron stars, PSR J0737–3039A and PSR J0737–3039B, completing a mildly eccentric orbit in 2.45 hr. A distinctive feature of such a system is that, at least for some years (2003-2008), both its components were simultaneously detectable as emitting radio pulsars. It is currently possible to collect pulses only from PSR J0737–3039A because the general relativistic geodetic precession (Damour & Ruffini 1974; Barker & O’Connell 1975) of the spin of PSR J0737–3039B, measured in 2008 by Breton et al. (2008) to a $\simeq 13\%$ accuracy, displaced its radio beam away from the line of sight. Since its discovery, PSR J0737–3039A/B turned out to be a unique laboratory to perform tests of relativistic gravity in a stronger regime than in our solar system (Kramer et al. 2006).

To the first order of its post-Newtonian (1pN) expansion, the General Theory of Relativity

(GTR) predicts, among other things, that the argument of periastron ω of the relative orbit of a gravitationally bound binary system made of two spinning bodies A and B with masses M_A , M_B and angular momenta \mathbf{S}^A , \mathbf{S}^B undergoes an orbit-averaged, long term variation made of two contributions. The first one, dubbed as “gravitoelectric” (Mashhoon 2001, 2003) and denoted here as $\dot{\omega}^{\text{GR}}$, depends only on the sum M of the masses of A and B. It is the generalization of the time-honored, formerly anomalous perihelion precession of Mercury in the field of the Sun explained by Einstein (1915) with his GTR, and reads (Robertson 1938; Damour & Schäfer 1988; Soffel 1989; Brumberg 1991)

$$\dot{\omega}^{\text{GR}} = \frac{3 n_b \mu}{c^2 a (1 - e^2)}. \quad (1)$$

In Equation (1), c is the speed of light in vacuum, $\mu \doteq GM$ is the gravitational parameter of the binary made of the product of the Newtonian constant of gravitation G times M , a and e are the semimajor axis and the eccentricity, respectively, of the relative orbit, while $n_b \doteq \sqrt{\mu/a^3}$ is the Keplerian mean motion.

The second general relativistic contribution to the 1pN periastron precession, dubbed as “gravitomagnetic” (Thorne, MacDonald & Price 1986; Thorne 1986, 1988; Mashhoon 2001; Rindler 2001; Mashhoon 2003) and denoted here as $\dot{\omega}^{\text{LT}}$, depends on both the masses and the spins of A and B, and is the generalization to the two-body case of the¹ Lense–Thirring effect, originally worked out by Lense & Thirring (1918); Mashhoon, Hehl & Theiss (1984) for a point particle orbiting a massive rotating primary, the orientation in space of whose spin is assumed to be known. For an arbitrary orientation in space of the spins of the binary’s components, also the inclination I and the node Ω experience long-term gravitomagnetic spin-orbit shifts. Contrary to what sometimes misrepresented in the literature (Hu et al. 2020), the only unquestioned test of gravitomagnetism performed, to date, in the weaker field of Earth was carried out with the dedicated space-based mission Gravity Probe B (GP-B) (Everitt 1974) measuring the Pugh-Schiff spin precessions (Pugh 1959; Schiff 1960) of four spaceborne gyroscopes to a 19 percent accuracy (Everitt et al. 2011, 2015) instead of the originally envisaged $\simeq 1$ percent (Everitt et al. 2001). The attempts to measure the Lense–Thirring orbital precessions with the Earth’s artificial satellites of the LAGEOS type (Ciufolini et al. 2013; Lucchesi et al. 2019, 2020) have always been controversial so far; see, e.g., Iorio et al. (2011); Renzetti (2013b,a, 2014), and references therein.

In principle, also the quadrupole mass moments Q^A , Q^B of A and B has an impact on the shifts of I , Ω and ω through formally Newtonian contributions² which, in the present case, will turn out to be negligible (Hu et al. 2020), as it will be independently confirmed here.

To the 2pN order, there is another gravitoelectric contribution to the periastron precession

¹According to the historical analyses by Pfister (2007, 2008, 2014), it should be dubbed, more appropriately, as Einstein–Thirring–Lense effect.

²In fact, the are of the order of $O(c^{-2})$ because of the relativistic expressions of the quadrupole mass moments of highly compact objects such as neutron stars.

depending only on the masses of A and B (Damour & Schäfer 1988; Schäfer & Wex 1993a,b); it will not be treated here.

The extraction of $\dot{\omega}^{\text{LT}}$ from the experimentally measured total periastron precession $\dot{\omega}_{\text{obs}}$ of PSR J0737–3039A/B, a possibility firstly envisaged by Lyne et al. (2004); Lattimer & Schutz (2005); Kramer et al. (2006), would allow to get important insights on the equation of state (EOS) of the dense matter inside neutron stars. Indeed, by assuming the validity of GTR, the knowledge of $\dot{\omega}^{\text{LT}}$ could be used to constrain the EOS through the determination of the moment of inertia (MOI) \mathcal{I}_A of PSR J0737–3039A. Conversely, if the MOI could be independently determined by other means, a test of the Lense–Thirring effect could be performed to some level of accuracy. In this respect, a necessary condition for the successful outcome of the aforementioned strategy is that the experimental error $\sigma_{\dot{\omega}_{\text{obs}}}$ in determining the periastron precession is adequately smaller than $\dot{\omega}^{\text{LT}}$. Furthermore, as quantitatively investigated for the first time by Iorio (2009), Equation (1) must be calculated with sufficient accuracy in order to be subtracted from $\dot{\omega}_{\text{obs}}$, acting as a source of major systematic uncertainty; see also the general discussion by Damour & Schäfer (1988) before the discovery of PSR J0737–3039A/B. The same holds also for the 2pN contribution to the periastron precession whose magnitude may be comparable to the 1pN gravitomagnetic one (Hu et al. 2020). To this aim, the masses of both the neutron stars must be independently and accurately determined. Recently, Hu et al. (2020) thoroughly investigated such aspects in view of the increasing amount of accurate pulsar timing data which will be collected from the MeerKAT and SKA facilities in the ongoing decade. For a previous analysis, see Kehl et al. (2017); Miao et al. (2021) dealt with binary pulsars with shorter orbital periods, yet to be discovered. Basing their analyses on the contribution to $\dot{\omega}^{\text{LT}}$ from PSR J0737–3039A only, Hu et al. (2020) concluded that a MOI measurement with 11 per cent accuracy (68 per cent confidence) would be possible by 2030. Conversely, by assuming a sufficiently accurate knowledge of the EOS by that date, Hu et al. (2020) suggested that a Lense–Thirring test accurate to the 7 per cent level could be feasible. Hu et al. (2020) neglected the contribution of \mathbf{S}^{B} to $\dot{\omega}^{\text{LT}}$ because of the much slower rotation of PSR J0737–3039B with respect to PSR J0737–3039A. Moreover, in considering only $\dot{\omega}^{\text{LT,A}}$, Hu et al. (2020) assumed \mathbf{S}^{A} exactly aligned with the orbital angular momentum \mathbf{L} .

The paper is organized as follows. In Section 2, such assumptions by Hu et al. (2020) are quantitatively checked in order to see if the full expression of $\dot{\omega}^{\text{LT}}$, compared with the expected future improvements in $\sigma_{\dot{\omega}_{\text{obs}}}$, will be, sooner or later, required in the timing of PSR J0737–3039A/B. In particular, the consequences on $\dot{\omega}^{\text{LT,A}}$ of the misalignment between \mathbf{L} and \mathbf{S}^{A} are treated in Section 2.1, while the contribution of \mathbf{S}^{B} to $\dot{\omega}^{\text{LT}}$ is evaluated in Section 2.2. The gravitomagnetic spin-orbit precessions of \mathbf{I} and $\mathbf{\Omega}$ are dealt with in Section 3: their upper bounds are calculated and compared with the current experimental uncertainties in determining such orbital elements. The long-term rates of change of \mathbf{I} , $\mathbf{\Omega}$ and $\boldsymbol{\omega}$ due to the quadrupole mass moments of A and B are worked out in Section 4. Section 5 summarizes the findings of the paper and offers concluding remarks.

Notations

Here, some basic notations and definitions used in the text are shown

G : Newtonian constant of gravitation

c : speed of light in vacuum

M_A : mass of PSR J0737–3039A

\mathcal{I}_A : moment of inertia (MOI) of PSR J0737–3039A

ν_A : spin frequency of PSR J0737–3039A

P_A : spin period of PSR J0737–3039A

Q_A : dimensional quadrupole mass moment of PSR J0737–3039A

S^A : spin angular momentum of PSR J0737–3039A

\hat{S}^A : unit vector of the spin angular momentum of PSR J0737–3039A

$S^A = \mathcal{I}_A 2\pi\nu_A$: magnitude of the spin angular momentum of PSR J0737–3039A

λ_A : angle between the reference z axis, directed along the line of sight away from the observer, and the spin axis of PSR J0737–3039A (Damour & Taylor 1992, Figure 1)

ψ_A : angle between the reference x axis and the projection of the spin axis of PSR J0737–3039A onto the plane of the sky, assumed as reference $\{x, y\}$ plane (Damour & Taylor 1992, Figure 1)

M_B : mass of PSR J0737–3039B

\mathcal{I}_B : moment of inertia (MOI) of PSR J0737–3039B

ν_B : spin frequency of PSR J0737–3039B

P_B : spin period of PSR J0737–3039B

Q_B : dimensional quadrupole mass moment of PSR J0737–3039B

S^B : spin angular momentum of PSR J0737–3039B

\hat{S}^B : unit vector of the spin angular momentum of PSR J0737–3039B

$S^B = \mathcal{I}_B 2\pi\nu_B$: magnitude of the spin angular momentum of PSR J0737–3039B

λ_B : angle between the reference z axis, directed along the line of sight away from the observer, and the spin axis of PSR J0737–3039B (Damour & Taylor 1992, Figure 1)

ψ_B : angle between the reference x axis and the projection of the spin axis of PSR J0737–3039B onto the plane of the sky, assumed as reference $\{x, y\}$ plane (Damour & Taylor 1992, Figure 1)

$M \doteq M_A + M_B$: total mass of PSR J0737–3039A/B

$\mu \doteq GM$: gravitational parameter of PSR J0737–3039A/B

a : semimajor axis of the relative orbit of PSR J0737–3039A/B

$n_b \doteq \sqrt{\mu/a^3}$: mean motion

$P_b \doteq 2\pi/n_b$: orbital period

$a_A = a M_B/M$: barycentric semimajor axis of PSR J0737–3039A

e : orbital eccentricity

L : orbital angular momentum

δ_A : misalignment angle between L and S^A

δ_B : misalignment angle between L and S^B

I : angle between the reference z axis, directed along the line of sight away from the observer, and the orbital angular momentum (Damour & Taylor 1992, Figure 1)

$x_A \doteq a_A \sin I/c$: projected semimajor axis of PSR J0737–3039A

Ω : longitude of the ascending node

$\eta_A \doteq \psi_A - \Omega$: angle between the projection of the spin axis of PSR J0737–3039A onto the plane of the sky and the longitude of the ascending node (Damour & Taylor 1992, Figure 1)

$\eta_B \doteq \psi_B - \Omega$: angle between the projection of the spin axis of PSR J0737–3039B onto the plane of the sky and the longitude of the ascending node (Damour & Taylor 1992, Figure 1)

$\mathbf{n} \doteq \{\sin I \sin \Omega, -\sin I \cos \Omega, \cos I\}$: unit vector of the orbital angular momentum

$\mathbf{l} \doteq \{\cos \Omega, \sin \Omega, 0\}$: unit vector directed along the line of the nodes towards the ascending node

$\mathbf{m} \doteq \{-\cos I \sin \Omega, \cos I \cos \Omega, \sin I\}$: unit vector in the orbital plane perpendicular to \mathbf{l} such that $\mathbf{l} \times \mathbf{m} = \mathbf{n}$.

ω : argument of periastron

For the numerical values of most of such quantities, see Kramer et al. (2006).

2. Using the periastron precession

In the following, the coordinate system of Figure 1 in Damour & Taylor (1992) will be adopted; its reference z axis is directed along the line of the sight away from the observer, while the reference $\{x, y\}$ plane is assumed coincident with the plane of the sky. Thus, the components of, say, $\hat{\mathbf{S}}^A$ can be parameterized in terms of the spherical angles λ_A, ψ_A as

$$\hat{S}_x^A = \sin \lambda_A \cos \psi_A, \quad (2)$$

$$\hat{S}_y^A = \sin \lambda_A \sin \psi_A, \quad (3)$$

$$\hat{S}_z^A = \cos \lambda_A. \quad (4)$$

The full analytical expression of the Lense–Thirring periastron precession of a two–body system whose spin angular momenta are arbitrarily oriented in space is (Iorio 2017)

$$\dot{\omega}^{\text{LT}} = -\frac{2 G S^A}{c^2 a^3 (1 - e^2)^{3/2}} \left(1 + \frac{3 M_B}{4 M_A}\right) \hat{\mathbf{S}}^A \cdot (2\mathbf{n} + \cot I \mathbf{m}) + A \Leftrightarrow B = \quad (5)$$

$$= -\frac{G S^A}{c^2 a^3 (1 - e^2)^{3/2}} \left(1 + \frac{3 M_B}{4 M_A}\right) [6 \cos I \cos \lambda_A + (3 \cos 2I - 1) \csc I \sin \lambda_A \sin \eta_A] + A \Leftrightarrow B. \quad (6)$$

For earlier, more or less explicit results, see, e.g., Kalitzin (1959), Michalska (1960), Damour & Schäfer (1988, Equations (5.11a)), Brumberg (1991, Section 4.4.4) and Wex (1995). Furthermore, in Barker & O’Connell (1975) the two-body Lense–Thirring orbital precessions are written in vectorial form. If $\hat{\mathbf{S}}^A$ and \mathbf{n} are exactly aligned, i.e. if

$$I = \lambda_A, \quad (7)$$

$$\eta_A = 270^\circ, \quad (8)$$

from Equation (6) one has

$$\dot{\omega}^{\text{LT}, A} = -\frac{4 G S^A}{c^2 a^3 (1 - e^2)^{3/2}} \left(1 + \frac{3 M_B}{4 M_A}\right). \quad (9)$$

2.1. The impact of the misalignment between \mathbf{S}^A and \mathbf{L}

Relying upon existing constraints on δ_A pointing towards a small misalignment between the orbital angular momentum and the spin axis of PSR J0737–3039A, Hu et al. (2020) based their

simulations on the assumption of an ideally perfect alignment between \mathbf{n} and $\hat{\mathbf{S}}^A$. Here, the impact on $\dot{\omega}^{\text{LT},A}$ of the departures from such a necessarily idealized condition will be quantitatively assessed.

About the MOI of PSR J0737–3039A, estimates for it were recently given in the literature; see Silva et al. (2021) and references therein. Relying upon such results, the value

$$\mathcal{I}_A = 1.6 \times 10^{38} \text{ kg m}^2 \quad (10)$$

is assumed here.

The misalignment angle δ_A is a function of I , λ_A , η_A defined by

$$\cos \delta_A = \mathbf{n} \cdot \hat{\mathbf{S}}^A = \cos I \cos \lambda_A - \sin I \sin \eta_A \sin \lambda_A. \quad (11)$$

According to Ferdman et al. (2013), who analysed the pulse profile shape over six years, it is close to zero, with an upper bound as little as

$$\delta_A \leq 3.2^\circ. \quad (12)$$

The bound of Equation (12) was inferred by assuming that the observed emission comes from both magnetic poles (Ferdman et al. 2013). By adopting the best estimate

$$I = 88.69^\circ \quad (13)$$

for the inclination angle from Kramer et al. (2006), it is possible to use Equation (11) and Equation (12) to constrain the spin's angles λ_A , η_A ; the allowed region in the plane $\{\lambda_A, \eta_A\}$ is displayed in Figure 1.

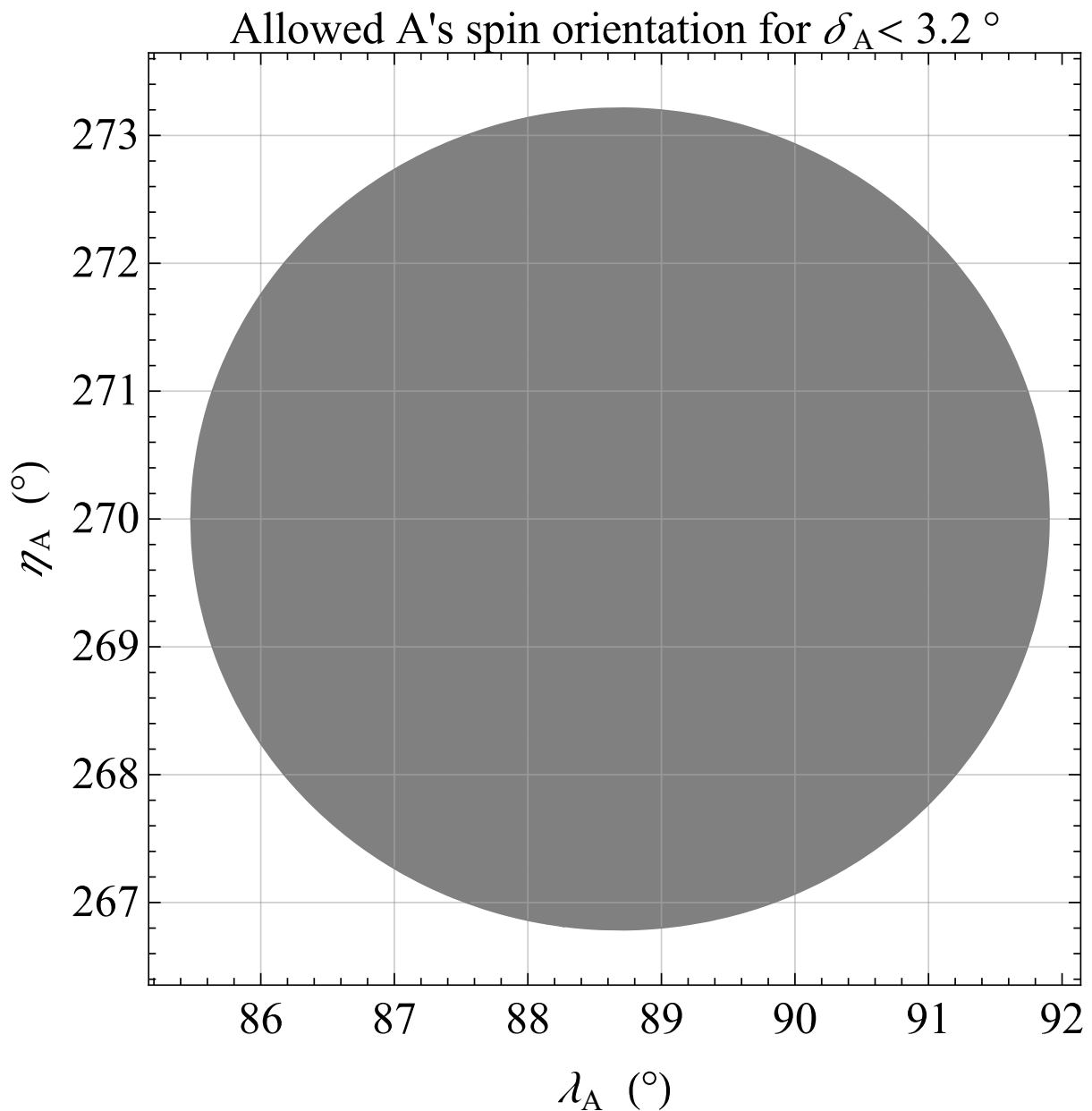


Fig. 1.— Allowed region, in the $\{\lambda_A, \eta_A\}$ plane, for the position angles λ_A, η_A of the spin S^A of PSR J0737–3039A. It was obtained by plotting δ_A , calculated with $I = 88.69^\circ$ (Kramer et al. 2006), as a function of λ_A, η_A according to Equation (11), and imposing the constraint of Equation (12).

It turns out that

$$85^\circ \lesssim \lambda_A \lesssim 92^\circ, \quad (14)$$

$$266^\circ \lesssim \eta_A \lesssim 274^\circ. \quad (15)$$

The Lense–Thirring periastron precession $\dot{\omega}^{\text{LT},A}$ due to S_A , calculated with Equation (6) and Equation (10), is plotted in Figure 2, in arcseconds per year ($'' \text{ yr}^{-1}$), as a function of λ_A , η_A restricted to the allowed region of Figure 1.

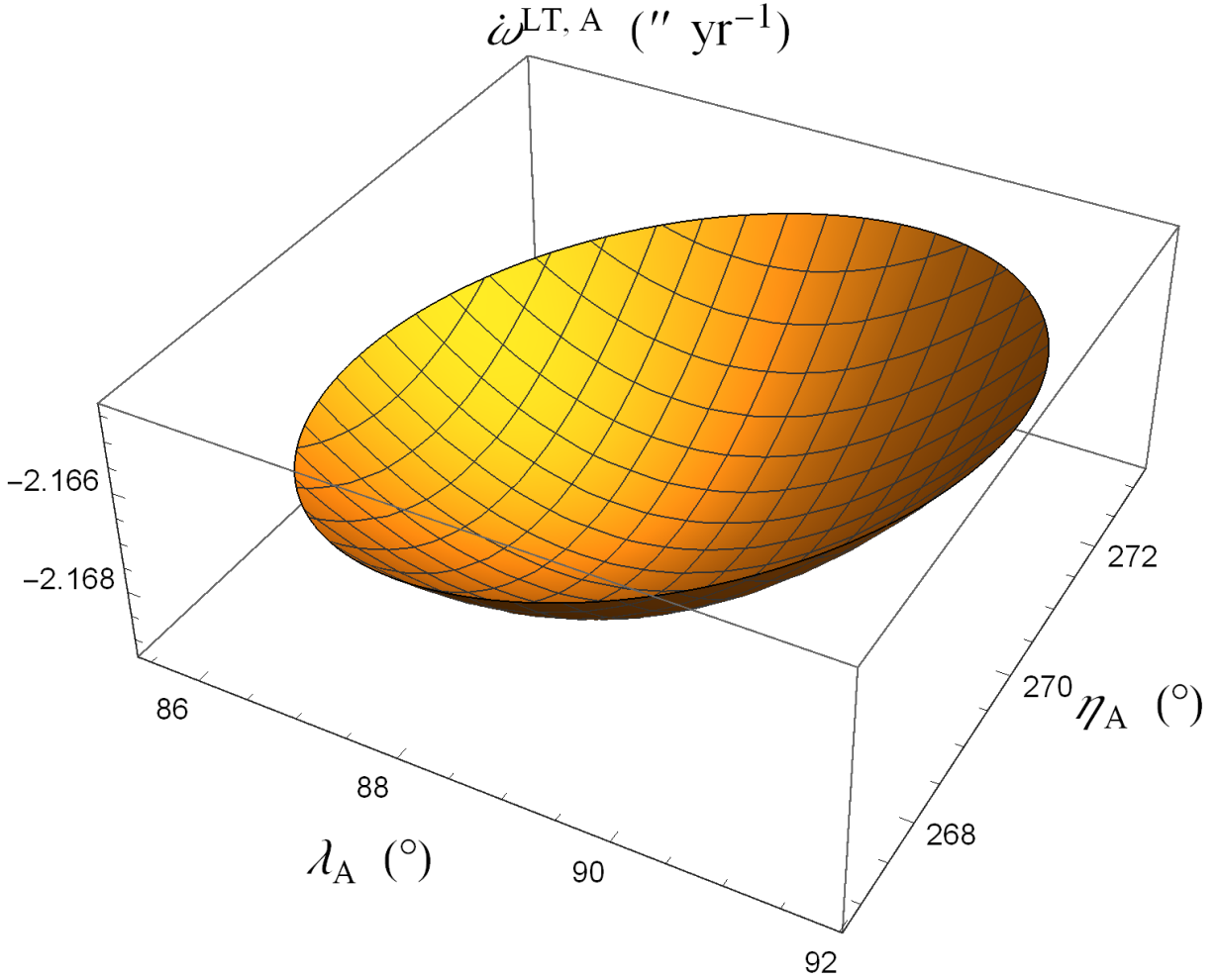


Fig. 2.— Plot of the Lense–Thirring periastron precession, in $'' \text{ yr}^{-1}$, due to S^A as a function of λ_A , η_A restricted to the allowed region of Figure 1. Equation (6) was used along with Equation (10) and the system’s values retrieved in Kramer et al. (2006).

It turns out that

$$-2.16928'' \text{ yr}^{-1} \leq \dot{\omega}^{\text{LT},A} \leq -2.16437'' \text{ yr}^{-1}, \quad (16)$$

corresponding to a range variation of

$$\Delta \dot{\omega}^{\text{LT},A} \doteq \dot{\omega}_{\text{max}}^{\text{LT},A} - \dot{\omega}_{\text{min}}^{\text{LT},A} = 0.00491'' \text{ yr}^{-1} = 8 \times 10^{-8} \dot{\omega}^{\text{GR}}. \quad (17)$$

Figure 2 of Hu et al. (2020) tells that the experimental uncertainty $\sigma_{\dot{\omega}_{\text{obs}}}$ in determining the periastron precession may reach the level of Equation (17) about after 2028, in the mid of the SKA 1-mid era.

2.2. The contribution of S^B

The contribution $\dot{\omega}^{\text{LT},B}$ due to S^B to the overall Lense–Thirring periastron precession can be obtained from Equation (6) with the exchange $A \leftrightarrow B$. Since the spin period of PSR J0737–3039B (Kramer et al. 2006)

$$P_B = 2.77 \text{ s} \quad (18)$$

is about 100 times longer than that of PSR J0737–3039A, Hu et al. (2020) neglected $\dot{\omega}^{\text{LT},B}$ in their analysis deeming it negligible.

Here, it will be quantitatively assessed by relying upon the current knowledge of the spin-orbit geometry of PSR J0737–3039B. The misalignment angle δ_B between L and S^B was accurately determined for the epoch 2 May 2006 by Breton et al. (2008) resulting equal to

$$128.79^\circ \leq \delta_B \leq 131.37^\circ \text{ (99.7\% confidence)}. \quad (19)$$

By using Equation (11) written for $A \rightarrow B$, Equation (19) permits to determine the allowed region in the $\{\lambda_B, \eta_B\}$ plane for the positional angles λ_B, η_B of \hat{S}^B . It is depicted in Figure 3.

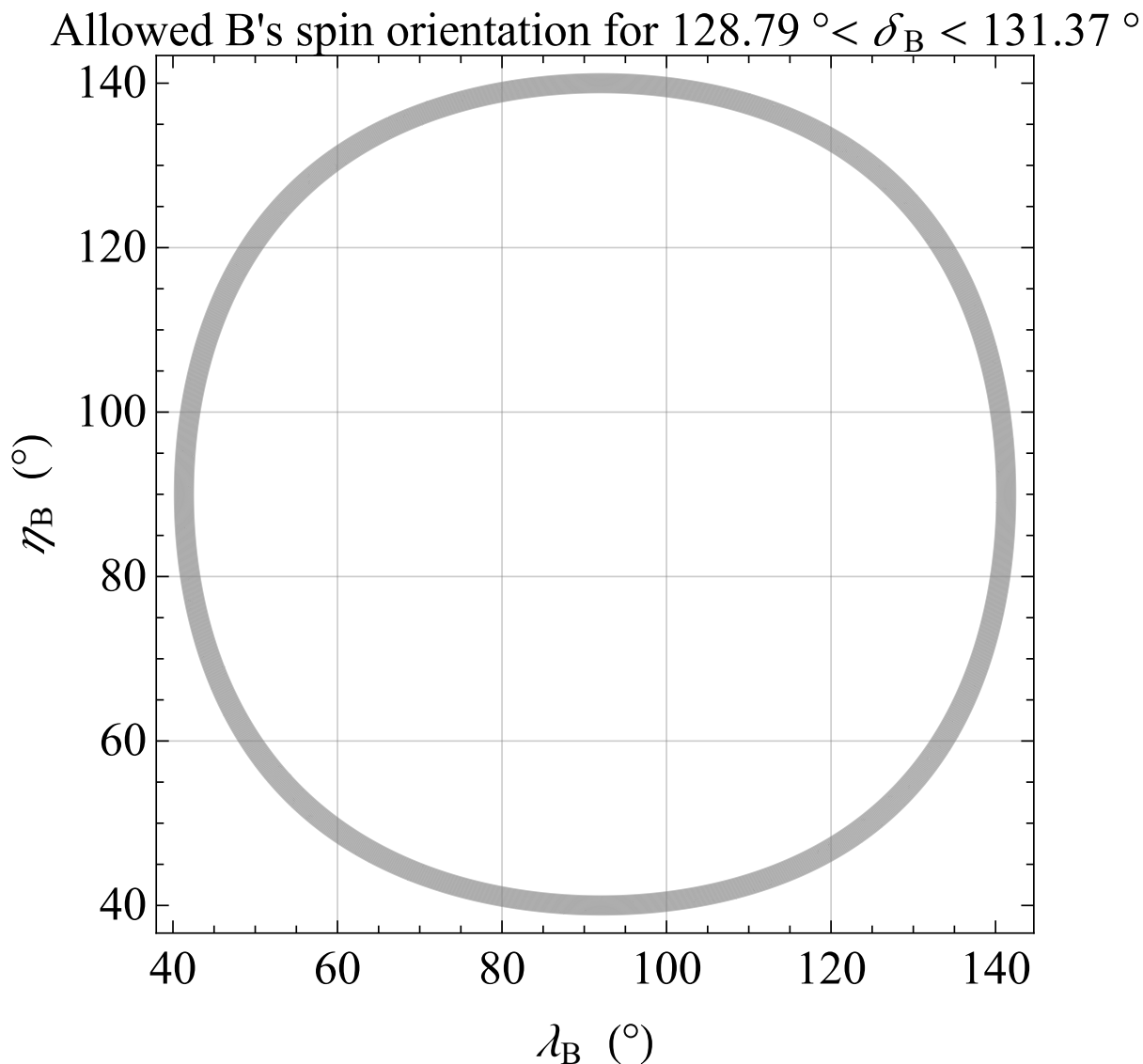


Fig. 3.— Allowed region, in the $\{\lambda_B, \eta_B\}$ plane, for the position angles λ_B, η_B of the spin S^B of PSR J0737–3039B. It was obtained by plotting δ_B , calculated with $I = 88.69^\circ$ (Kramer et al. 2006), as a function of λ_B, η_B according to Equation (11) with $A \rightarrow B$, and imposing the constraint of Equation (19) determined for the epoch 2 May 2006 by Breton et al. (2008).

It turns out to be a narrow annular region enclosed in a square $40^\circ \times 140^\circ$ wide. Figure 4 shows the corresponding $\dot{\omega}^{\text{LT},B}$ calculated for $\mathcal{I}_B = \mathcal{I}_A$.

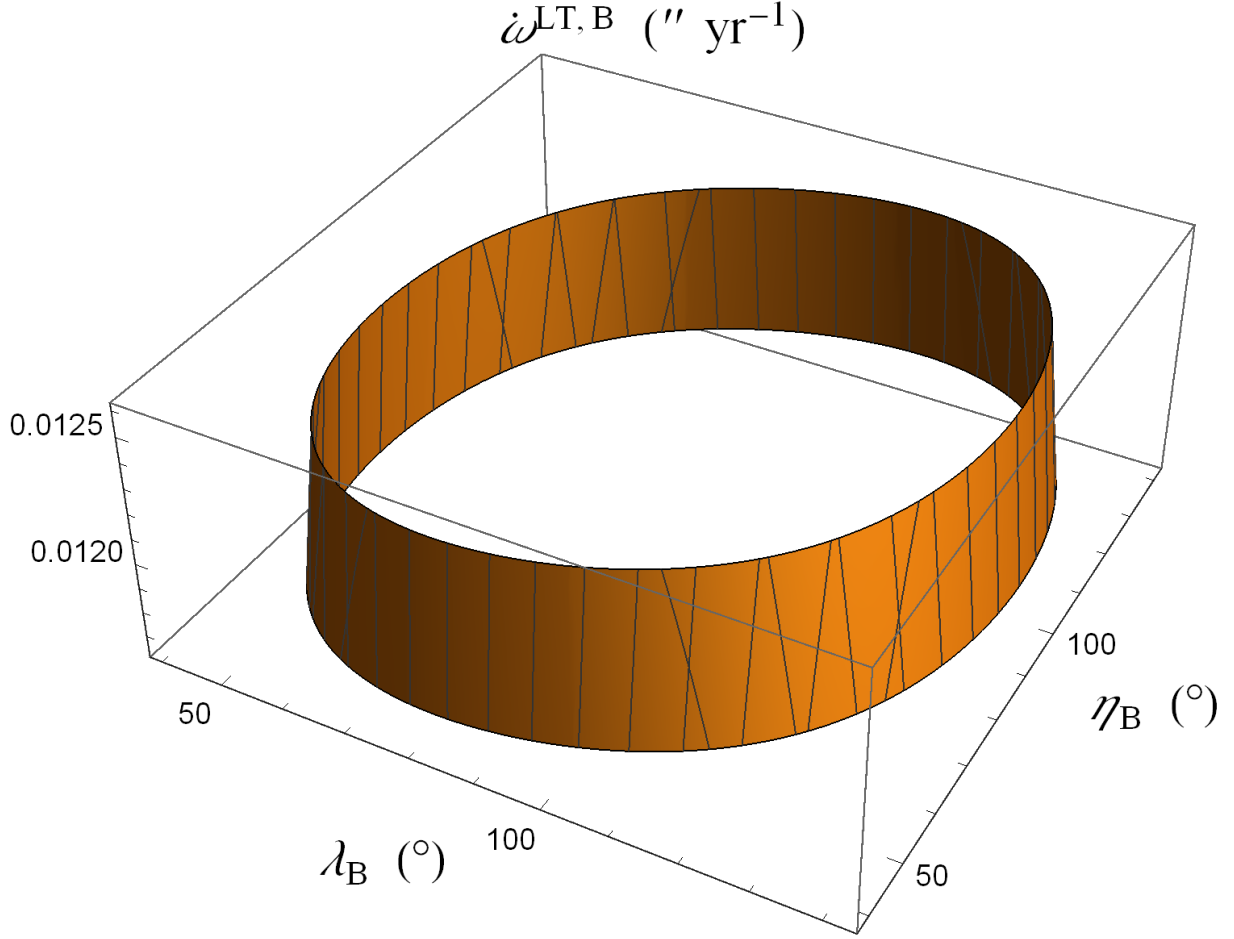


Fig. 4.— Plot of the Lense–Thirring periastron precession $\dot{\omega}^{\text{LT},\text{B}}$, in $'' \text{yr}^{-1}$, due to \mathcal{S}^{B} as a function of λ_{B} , η_{B} restricted to the allowed region of Figure 3. Equation (6) was used with the replacement $A \Leftrightarrow B$ along with Equation (10) and the system’s values retrieved in Kramer et al. (2006).

It turns out that

$$0.0116'' \text{yr}^{-1} \leq \dot{\omega}^{\text{LT},\text{B}} \leq 0.0126'' \text{yr}^{-1}, \quad (20)$$

corresponding to

$$\dot{\omega}^{\text{LT},\text{B}} \simeq 2 \times 10^{-7} \dot{\omega}^{\text{GR}}. \quad (21)$$

According to Figure 2 of Hu et al. (2020), $\sigma_{\dot{\omega}_{\text{obs}}}$ may reach the level of Equation (21) between the end of the MeerKAT+ era and the beginning of the SKA 1-mid phase about around 2025.

3. The spin-orbit precessions of the inclination and the node

According to Kramer et al. (2021), PSR J0737–3039A/B is one of the few binary pulsars for which I and Ω can be uniquely determined by means of long term monitoring of the interstellar scintillation following a strategy put forth for the first time by Lyne (1984); see, e.g., the determinations of I and³ Ω by Rickett et al. (2014). Nonetheless, further investigations are required to assess if the results from the scintillation method are consistent with those obtained from the standard pulsar timing including the Rotating Vector Model (RVM) (Kramer et al. 2021).

Thus, the gravitomagnetic spin-orbit rates of I and Ω are accurately calculated in order to check if a possible future measurement of them may be viable. It is important to stress that, contrary to the periastron, neither the inclination nor the node undergo 1pN+2pN mass-dependent gravitoelectric shifts. Their full spin-orbit rates can be explicitly expressed as (Iorio 2017)

$$\begin{aligned} \dot{I}^{\text{LT}} &= \frac{2GS^{\text{A}}}{c^2 a^3 (1-e^2)^{3/2}} \left(1 + \frac{3M_{\text{B}}}{4M_{\text{A}}}\right) \hat{\mathbf{S}}^{\text{A}} \cdot \mathbf{l} + \text{A} \Leftrightarrow \text{B} = \\ &= \frac{2GS^{\text{A}}}{c^2 a^3 (1-e^2)^{3/2}} \left(1 + \frac{3M_{\text{B}}}{4M_{\text{A}}}\right) \cos \eta_{\text{A}} \sin \lambda_{\text{A}} + \text{A} \Leftrightarrow \text{B}, \end{aligned} \quad (22)$$

$$\begin{aligned} \dot{\Omega}^{\text{LT}} &= \frac{2GS^{\text{A}}}{c^2 a^3 \sin I (1-e^2)^{3/2}} \left(1 + \frac{3M_{\text{B}}}{4M_{\text{A}}}\right) \hat{\mathbf{S}}^{\text{A}} \cdot \mathbf{m} + \text{A} \Leftrightarrow \text{B} = \\ &= \frac{2GS^{\text{A}}}{c^2 a^3 (1-e^2)^{3/2}} \left(1 + \frac{3M_{\text{B}}}{4M_{\text{A}}}\right) (\cos \lambda_{\text{A}} + \cot I \sin \eta_{\text{A}} \sin \lambda_{\text{A}}) + \text{A} \Leftrightarrow \text{B}. \end{aligned} \quad (23)$$

For more or less general expressions of the two-body Lense–Thirring out-of-plane orbital precessions, see also Michalska (1960), Damour & Schäfer (1988, Equations (5.11b)-(5.11c)), Brumberg (1991, Section 4.4.4) and Damour & Taylor (1992, Equation (3.27)). Moreover, Barker & O’Connell (1975) expressed the two-body Lense–Thirring orbital precessions in vectorial form.

Figure 5 displays the Lense–Thirring precessions $\dot{I}^{\text{LT,A}}$, $\dot{I}^{\text{LT,B}}$, $\dot{\Omega}^{\text{LT,A}}$, $\dot{\Omega}^{\text{LT,B}}$ calculated by means of Equations (22)-(23) within the allowed regions for $\hat{\mathbf{S}}^{\text{A}}$ and $\hat{\mathbf{S}}^{\text{B}}$, respectively, in the planes $\{\lambda_{\text{A}}, \eta_{\text{A}}\}$ and $\{\lambda_{\text{B}}, \eta_{\text{B}}\}$.

³Rickett et al. (2014) used a different convention for the node, which was accounted for by Hu et al. (2020, p. 3121) in releasing their result for Ω .

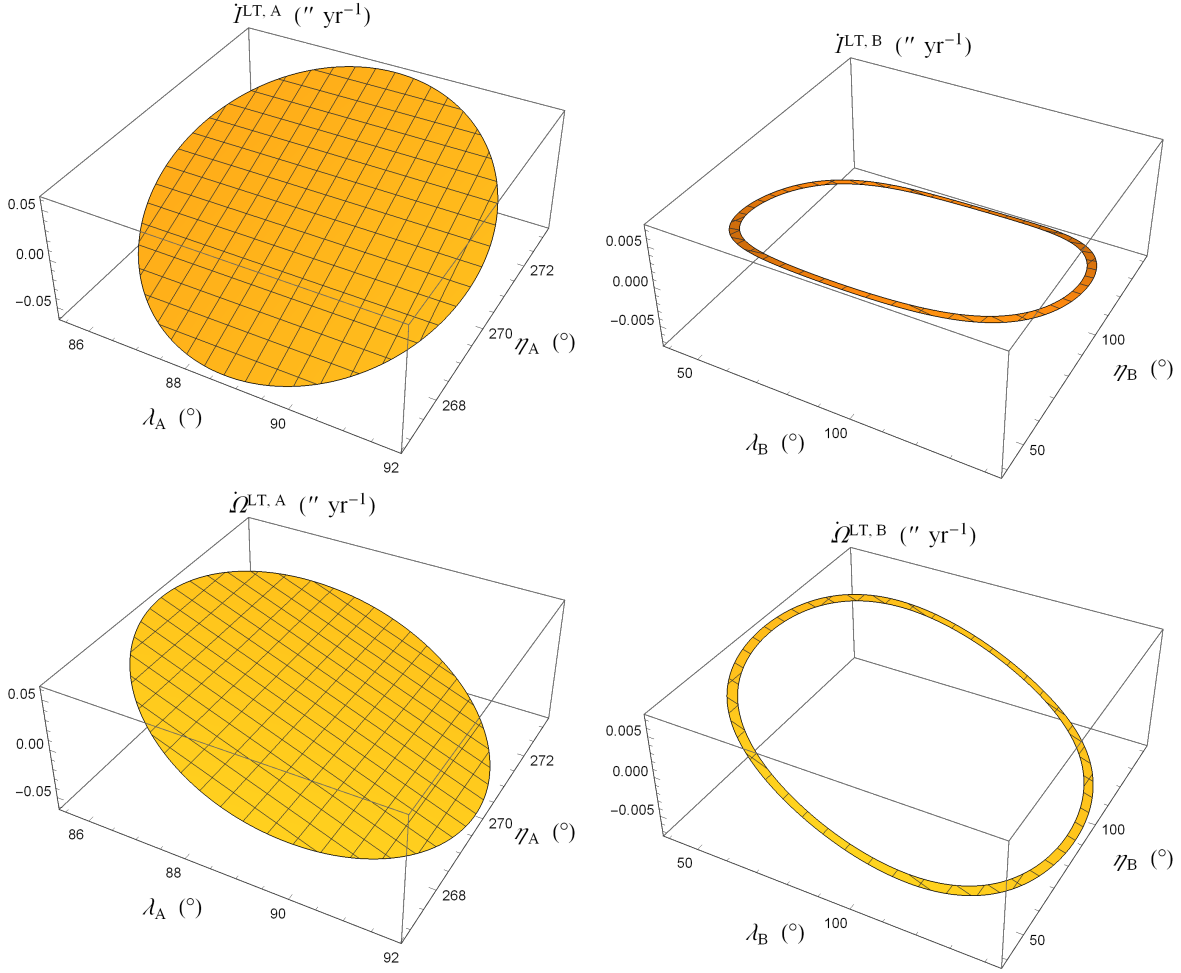


Fig. 5.— Plot of the Lense–Thirring inclination and node precessions $i^{LT,A}$, $i^{LT,B}$, $\dot{\Omega}^{LT,A}$, $\dot{\Omega}^{LT,B}$, in $'' \text{yr}^{-1}$, due to S^A and S^B as functions of λ_A , η_A and λ_B , η_B , respectively, restricted to the allowed regions of Figure 1 and Figure 3. Equations (22)-(23) were used along with Equation (10) for the moments of inertia and the system’s values retrieved in Kramer et al. (2006).

It turns out that the maximum size of the absolute value of the precessions due to the spin of PSR J0737–3039A is

$$|i^{LT,A}| \simeq |\dot{\Omega}^{LT,A}| \lesssim 0.05'' \text{yr}^{-1}, \quad (24)$$

while for the rates induced by PSR J0737–3039B the upper bound is

$$|i^{LT,B}| \simeq |\dot{\Omega}^{LT,B}| \lesssim 0.005'' \text{yr}^{-1}. \quad (25)$$

Furthermore, for some particular orientations of \hat{S}^A , \hat{S}^B , they can even vanish. The current experimental errors in determining I and Ω with the scintillation technique are several orders of

magnitude larger than Equations (24)-(25); suffice it to say that Rickett et al. (2014) report

$$\sigma_{I_{\text{obs}}} = 0.5^\circ, \quad (26)$$

$$\sigma_{\Omega_{\text{obs}}} = 2^\circ \quad (27)$$

over a time span of 1.5 yr.

As far as the gravitomagnetic spin-orbit precession of the inclination is concerned, another possibility to measure it consists, in principle, in determining the rate of change

$$\dot{x}_A = x_A \cot I \dot{I} = \frac{a_A \cos I}{c} \dot{I} \quad (28)$$

of the projected semimajor axis x_A of PSR J0737–3039A. Figure 6 shows $x_A^{\text{LT},A}$ as a function of λ_A, η_A restricted to their allowed region of Figure 1.

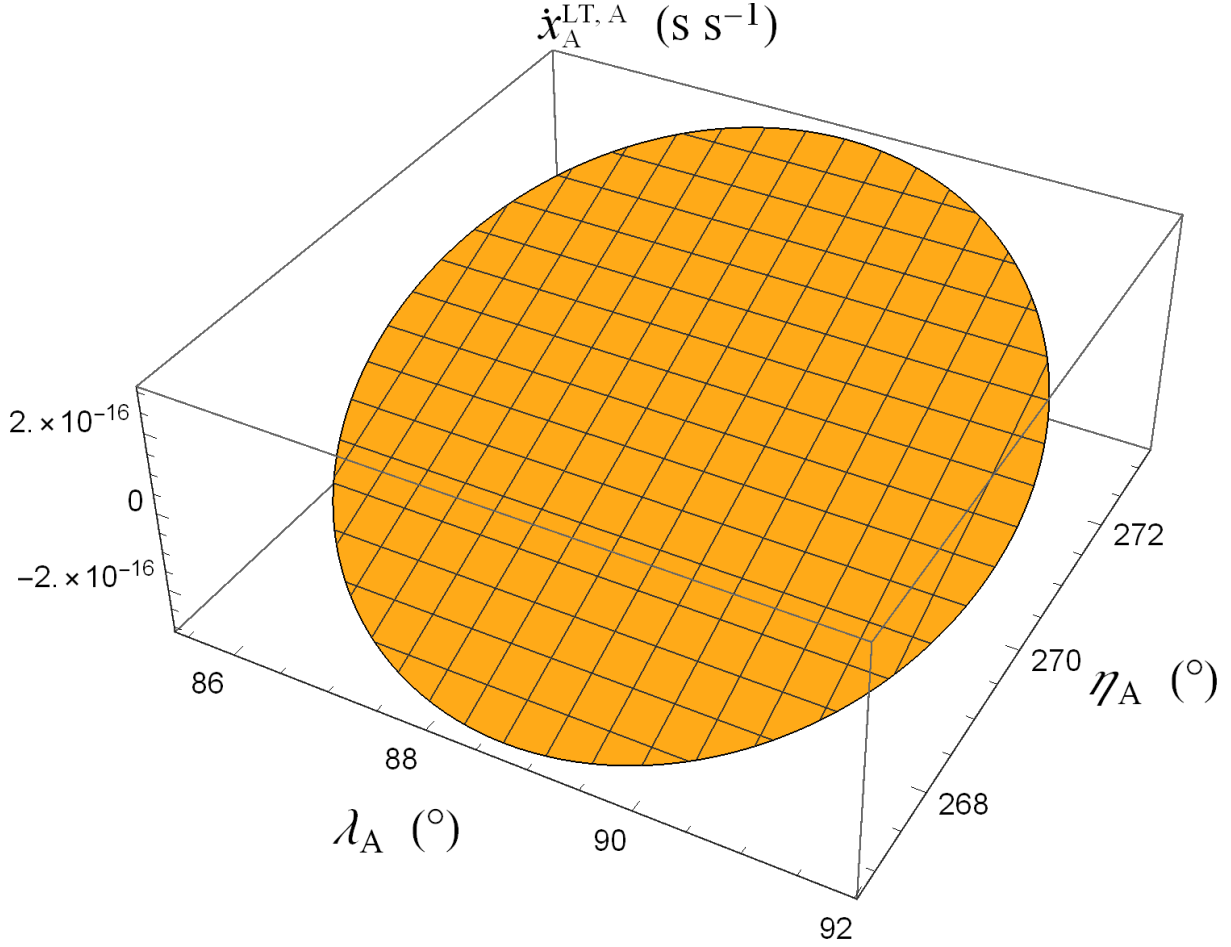


Fig. 6.— Plot of the Lense–Thirring rate of change $\dot{x}_A^{LT,A}$ of the projected semimajor axis x_A of PSR J0737–3039A, in s s^{-1} , due to S^A as a function of λ_A , η_A restricted to the allowed region of Figure 1. Equation (22) was used along with Equation (10) and the system’s values retrieved in Kramer et al. (2006).

The resulting maximum value of the size of the Lense–Thirring rate of change $\dot{x}_A^{LT,A}$ of the projected semimajor axis of PSR J0737–3039A is

$$|\dot{x}_A^{LT,A}| \lesssim 2 \times 10^{-16} \text{ s s}^{-1}. \quad (29)$$

Note that, for certain values of λ_A , η_A , $\dot{x}_A^{LT,A}$ vanishes. Despite, to date, measurements of \dot{x}_A are seemingly missing in the literature, a guess on the potentially achievable accuracy in its determination may be inferred from the published results. From (Kramer et al. 2006)

$$\sigma_{x_A^{\text{obs}}} = 1 \times 10^{-6} \text{ s} \quad (30)$$

over a time span of (Kramer et al. 2006)

$$\Delta t = 2.5 \text{ yr} = 7.88 \times 10^7 \text{ s}, \quad (31)$$

a plausible estimate of the accuracy in determining \dot{x}_A can be tentatively argued, amounting to

$$\sigma_{\dot{x}_A^{\text{obs}}} \simeq 1.2 \times 10^{-14} \text{ s s}^{-1}. \quad (32)$$

It should be remarked that Equation (32) is just two orders of magnitude larger than Equation (29); thus, it does not seem unreasonable to expect that a measurement of $\dot{x}_A^{\text{LT},A}$ may become feasible in the near future.

A binary system for which the Lense–Thirring rate of the projected semimajor axis seems to be measurable in the forthcoming years is PSR J1757–1854 (Cameron et al. 2018). For its pulsar p, by assuming (Lattimer & Schutz 2005)

$$\mathcal{I}_p = 1.2 \times 10^{38} \text{ kg m}^2, \quad (33)$$

one has (Cameron et al. 2018)

$$\dot{x}_p^{\text{LT}} \simeq 1.9 \times 10^{-14} \text{ s s}^{-1}. \quad (34)$$

Cameron et al. (2018) reported an experimental uncertainty in determining x_p

$$\sigma_{x_p} = 5 \times 10^{-6} \text{ s} \quad (35)$$

over an observational time span

$$\Delta t = 1.6 \text{ yr} = 5.05 \times 10^7 \text{ s}, \quad (36)$$

corresponding to a possible error in measuring \dot{x}_p of the order of

$$\sigma_{\dot{x}_p} \simeq 9.9 \times 10^{-14} \text{ s s}^{-1}. \quad (37)$$

Probably relying upon an analogous guess, Cameron et al. (2018) concluded that a measurement of Equation (34) to within 3σ would be possible in the following 8-9 years.

4. The quadrupole-induced orbital precessions

In principle, for an arbitrary orientation in space of $\hat{\mathbf{S}}^A$ and $\hat{\mathbf{S}}^B$, I , Ω and ω undergo Newtonian long-term rates of change due to the quadrupole mass moments Q^A , Q^B of A and B. Their explicit

general expressions are (Iorio 2017)

$$i^{\mathcal{Q}} = \frac{3 n_b Q_A}{2 a^2 (1 - e^2)^2 M_A} \left(\hat{\mathbf{S}}^A \cdot \mathbf{l} \right) \left(\hat{\mathbf{S}}^A \cdot \mathbf{n} \right) + A \Leftrightarrow B = \quad (38)$$

$$= \frac{3 n_b Q_A}{2 a^2 (1 - e^2)^2 M_A} \cos \eta_A \sin \lambda_A (\cos I \cos \lambda_A - \sin I \sin \eta_A \sin \lambda_A) + A \Leftrightarrow B, \quad (39)$$

$$\begin{aligned} \dot{\Omega}^{\mathcal{Q}} &= \frac{3 n_b Q_A \csc I}{2 a^2 (1 - e^2)^2 M_A} \left(\hat{\mathbf{S}}^A \cdot \mathbf{m} \right) \left(\hat{\mathbf{S}}^A \cdot \mathbf{n} \right) + A \Leftrightarrow B = \\ &= \frac{3 n_b Q_A}{4 a^2 (1 - e^2)^2 M_A} \left[2 \cos I (\cos^2 \lambda_A - \sin^2 \eta_A \sin^2 \lambda_A) + \right. \\ &\quad \left. + \cos 2I \csc I \sin \eta_A \sin 2\lambda_A \right] + A \Leftrightarrow B, \end{aligned} \quad (40)$$

$$\begin{aligned} \dot{\omega}^{\mathcal{Q}} &= -\frac{3 n_b Q_A}{4 a^2 (1 - e^2)^2 M_A} \left\{ 2 - 3 \left[\left(\hat{\mathbf{S}}^A \cdot \mathbf{l} \right)^2 + \left(\hat{\mathbf{S}}^A \cdot \mathbf{m} \right)^2 \right] + \right. \\ &\quad \left. + 2 \cot I \left(\hat{\mathbf{S}}^A \cdot \mathbf{m} \right) \left(\hat{\mathbf{S}}^A \cdot \mathbf{n} \right) \right\} + A \Leftrightarrow B = \\ &= \frac{3 n_b Q_A}{32 a^2 (1 - e^2)^2 M_A} \left[- (3 + 5 \cos 2I) (1 + 3 \cos 2\lambda_A) + \right. \\ &\quad \left. + 2 (1 - 5 \cos 2I) \cos 2\eta_A \sin^2 \lambda_A + \right. \\ &\quad \left. + 2 (\cos I - 5 \cos 3I) \csc I \sin \eta_A \sin 2\lambda_A \right] + A \Leftrightarrow B. \end{aligned} \quad (41)$$

See also Barker & O’Connell (1975) for their effects in vectorial form. References like, e.g., Smarr & Blandford (1976); Wex (1998) dealing with the orbital elements are either valid only for the restricted two-body case or are restricted to some particular spin-orbit geometry.

Hu et al. (2020), relying upon the relations by Bauböck et al. (2013) to calculate Q^A , claimed that

$$\dot{\omega}^{\mathcal{Q},A} \simeq 0.0001'' \text{ yr}^{-1} = 1.7 \times 10^{-9} \dot{\omega}^{\text{GR}}, \quad (42)$$

which would be likely negligible in the foreseeable future. Here, an independent evaluation will be offered in light of Equations (38)-(41) and of the most recent results in determining the key physical parameters of neutron stars in a rather EOS-independent way (Silva et al. 2021).

According to Silva et al. (2021), the dimensional quadrupole mass moment of a neutron star like PSR J0737–3039A can be expressed as

$$Q_A = -\bar{Q}_A \frac{M_A^3 G^2 \chi_A^2}{c^4}, \quad (43)$$

where \bar{Q}_A and χ_A are dimensionless parameters related to the MOI; Equation (43) is rather insensitive to the EOS (Silva et al. 2021). In particular,

$$\chi_A \doteq \frac{2\pi\nu_A M_A G \bar{I}_A}{c^3}, \quad (44)$$

where the dimensionless MOI-type parameter is defined as

$$\bar{I}_A = \frac{c^4 I_A}{M_A^3 G^2}. \quad (45)$$

Inserting Equations (44)-(45) in Equation (43), the quadrupole mass moment of PSR J0737–3039A can be written as

$$Q_A = -\bar{Q}_A \frac{4\pi^2 \nu_A^2 I_A^2}{c^2 M_A}. \quad (46)$$

Silva et al. (2021) provided estimates of the moment of inertia I_A of PSR J0737–3039A, and of the dimensionless parameter

$$\bar{Q}_\star \simeq 6 \quad (47)$$

for the isolated millisecond pulsar PSR J0030+0451 whose spin frequency $\nu_\star = 205.53$ Hz is about five times higher than that of PSR J0737–3039A. By calculating Equation (46) for PSR J0737–3039A, it is possible to obtain

$$Q_A = -\bar{Q}_A 8 \times 10^{33} \text{ kg m}^2. \quad (48)$$

Equation (48) is comparable to the value calculated by Iorio (2017, Equations (88)-(89)) relying upon Laarakkers & Poisson (1999).

Incidentally, Equation (46) yields for PSR J0737–3039B a value four orders of magnitude smaller than Equation (48).

By calculating Equation (41) with, say, Equation (47) in Equation (48), its plot in the allowed region of Equations (14)-(15) for λ_A , η_A , returns

$$\dot{\omega}^{Q,A} \simeq 0.00017'' \text{ yr}^{-1}, \quad (49)$$

in agreement with Equation (42).

As far as the other orbital elements are concerned, it turns out that

$$|\dot{I}^{Q,A}| \lesssim 5 \times 10^{-6} \text{'' yr}^{-1}, \quad (50)$$

$$|\dot{\Omega}^{Q,A}| \lesssim 5 \times 10^{-6} \text{'' yr}^{-1}, \quad (51)$$

$$|\dot{x}_A^{Q,A}| \lesssim 4 \times 10^{-20} \text{ s s}^{-1}. \quad (52)$$

Such so small figures are likely negligible, from an observational point of view, in any foreseeable future.

5. Summary and conclusions

The expected improvements in the experimental accuracy $\sigma_{\dot{\omega}_{\text{obs}}}$ in determining the periastron precession $\dot{\omega}$ of PSR J0737–3039A/B, which, in units of the general relativistic mass-only gravitoelectric precession $\dot{\omega}^{\text{GR}}$, may reach the $\simeq 10^{-7} - 10^{-8} \dot{\omega}^{\text{GR}}$ level by 2030 thanks to the SKA 1-mid facility, requires a careful modeling of all the dynamical contributions to the long-term rate of change of such an orbital element.

Among them, there is the general relativistic gravitomagnetic Lense–Thirring periastron rate $\dot{\omega}^{\text{LT}}$, that is dominated by the contribution $\dot{\omega}^{\text{LT},A}$ induced by the spin angular momentum \mathbf{S}^A of PSR J0737–3039A, assumed aligned with the orbital angular momentum \mathbf{L} . It is particularly important since it depends on the pulsar’s moment of inertia \mathcal{I}_A whose determination can give valuable information on the equation of state of the ultradense matter inside neutron stars.

Here, it was demonstrated that neglecting the part of $\dot{\omega}^{\text{LT},A}$ due to the misalignment between \mathbf{S}^A and \mathbf{L} , which corresponds to an allowed orientation in space of $\hat{\mathbf{S}}^A$ constrained within $85^\circ \lesssim \lambda_A \lesssim 92^\circ$, $266^\circ \lesssim \eta_A \lesssim 274^\circ$, would introduce an error which may be as large as $\Delta\dot{\omega}^{\text{LT},A} \simeq 8 \times 10^{-8} \dot{\omega}^{\text{GR}}$. Furthermore, also the contribution $\dot{\omega}^{\text{LT},B}$ to $\dot{\omega}^{\text{LT}}$ from the spin \mathbf{S}^B of PSR J0737–3039B, always neglected in all the analyses published so far, should be taken into account since its magnitude may be as large as $\dot{\omega}^{\text{LT},B} \simeq 2 \times 10^{-7} \dot{\omega}^{\text{GR}}$.

Also the orbital inclination I and the node Ω undergo Lense–Thirring precessions whose sizes, for PSR J0737–3039A/B, are of the order of $|\dot{I}^{\text{LT}}| \simeq |\dot{\Omega}^{\text{LT}}| \lesssim 0.05$ arcseconds per year. The current experimental uncertainty in measuring I and Ω of PSR J0737–3039A/B with the scintillation technique is several orders of magnitude larger. Should the rate \dot{x}_A of the projected semimajor axis x_A of PSR J0737–3039A be measurable, the size of its expected gravitomagnetic spin-orbit contribution is $|\dot{x}_A^{\text{LT}}| \lesssim 2 \times 10^{-16} \text{ s s}^{-1}$. The experimental uncertainty $\sigma_{\dot{x}_A^{\text{obs}}}$ in measuring \dot{x}_A , hypothesized on the basis of the data released in 2006, is of the order of $\simeq 10^{-14} \text{ s s}^{-1}$.

The contribution to $\dot{\omega}$ by the quadrupole mass moment Q^A of PSR J0737–3039A, is confirmed to be likely negligible in the foreseeable future since it is as little as $\dot{\omega}^{Q,A} \simeq 10^{-9} \dot{\omega}^{\text{GR}}$.

Data availability

No new data were generated or analysed in support of this research.

REFERENCES

- Barker B. M., O’Connell R. F., 1975, *Phys. Rev. D*, 12, 329
- Bauböck M., Berti E., Psaltis D., Özel F., 2013, *ApJ*, 777, 68
- Breton R. P. et al., 2008, *Science*, 321, 104
- Brumberg V. A., 1991, *Essential Relativistic Celestial Mechanics*. Adam Hilger, Bristol
- Burgay M. et al., 2003, *Nature*, 426, 531
- Cameron A. D. et al., 2018, *MNRAS*, 475, L57
- Ciufolini I. et al., 2013, *Nuclear Physics B Proceedings Supplements*, 243, 180
- Damour T., Ruffini R., 1974, *C.R. Acad. Sc. Paris, Série A*, 279, 971
- Damour T., Schäfer G., 1988, *Nuovo Cimento B*, 101, 127
- Damour T., Taylor J. H., 1992, *Phys. Rev. D*, 45, 1840
- Einstein A., 1915, *Sitzungsber. Kön. Preuß. Akad. Wiss. zu Berlin*, 831–839
- Everitt C. W. F., 1974, in *Proceedings of the International School of Physics “Enrico Fermi”. Course LVI. Experimental Gravitation*, Bertotti B., ed., Academic Press, New York and London, pp. 331–360
- Everitt C. W. F., Buchman S., Debra D. B., Keiser G. M., Lockhart J. M., Muhlfelder B., Parkinson B. W., Turneare J. P., 2001, in *Lecture Notes in Physics*, Berlin Springer Verlag, Vol. 562, Gyros, Clocks, Interferometers ...: Testing Relativistic Gravity in Space, Lämmerzahl C., Everitt C. W. F., Hehl F. W., eds., p. 52
- Everitt C. W. F. et al., 2011, *Phys. Rev. Lett.*, 106, 221101
- Everitt C. W. F. et al., 2015, *Class. Quantum Gravity*, 32, 224001
- Ferdman R. D. et al., 2013, *ApJ*, 767, 85
- Hu H., Kramer M., Wex N., Champion D. J., Kehl M. S., 2020, *MNRAS*, 497, 3118
- Iorio L., 2009, *New A*, 14, 40
- Iorio L., 2017, *Eur. Phys. J. C*, 77, 439
- Iorio L., Lichtenegger H. I. M., Ruggiero M. L., Corda C., 2011, *Ap&SS*, 331, 351
- Kalitzin N. S., 1959, *N. Cimento*, 11, 178

- Kehl M. S., Wex N., Kramer M., Liu K., 2017, in *The Fourteenth Marcel Grossmann Meeting. Proceedings of the MG14 Meeting on General Relativity*, Bianchi M., Jantzen R., Ruffini R., eds., World Scientific, Singapore, pp. 1860–1865
- Kramer M. et al., 2006, *Science*, 314, 97
- Kramer M. et al., 2021, *MNRAS*, 504, 2094
- Laarakkers W. G., Poisson E., 1999, *ApJ*, 512, 282
- Lattimer J. M., Schutz B. F., 2005, *ApJ*, 629, 979
- Lense J., Thirring H., 1918, *PhyZ*, 19, 156
- Lucchesi D., Visco M., Peron R., Bassan M., Pucacco G., Pardini C., Anselmo L., Magnafico C., 2020, *Universe*, 6, 139
- Lucchesi D. M., Anselmo L., Bassan M., Magnafico C., Pardini C., Peron R., Pucacco G., Visco M., 2019, *Universe*, 5, 141
- Lyne A. G., 1984, *Nature*, 310, 300
- Lyne A. G. et al., 2004, *Science*, 303, 1153
- Mashhoon B., 2001, in *Reference Frames and Gravitomagnetism*, Pascual-Sánchez J. F., Floría L., San Miguel A., Vicente F., eds., World Scientific, Singapore, pp. 121–132
- Mashhoon B., 2003, in *The Measurement of Gravitomagnetism: A Challenging Enterprise*, Iorio L., ed., Nova Science Publishers, Hauppauge (NY), pp. 29–39
- Mashhoon B., Hehl F. W., Theiss D. S., 1984, *General Relativity and Gravitation*, 16, 727
- Miao X., Xu H., Shao L., Liu C., Ma B.-Q., 2021, arXiv e-prints, arXiv:2107.05812
- Michalska R., 1960, *Bull. Acad. Polon. Sci., Ser. Math. Astr. Phys.*, 8, 247
- Pfister H., 2007, *General Relativity and Gravitation*, 39, 1735
- Pfister H., 2008, in *The Eleventh Marcel Grossmann Meeting On Recent Developments in Theoretical and Experimental General Relativity, Gravitation and Relativistic Field Theories*, Kleinert H., Jantzen R. T., Ruffini R., eds., World Scientific, Singapore, pp. 2456–2458
- Pfister H., 2014, in *Springer Proceedings in Physics, Vol. 157, Relativity and Gravitation*, Bičák J., Ledvinka T., eds., Springer Verlag, Berlin/Heidelberg, pp. 191–197

- Pugh G., 1959, Proposal for a Satellite Test of the Coriolis Prediction of General Relativity. Research Memorandum 11, Weapons Systems Evaluation Group, The Pentagon, Washington D.C.
- Renzetti G., 2013a, *New A*, 23, 63
- Renzetti G., 2013b, *Central European Journal of Physics*, 11, 531
- Renzetti G., 2014, *New A*, 29, 25
- Rickett B. J. et al., 2014, *ApJ*, 787, 161
- Rindler W., 2001, *Relativity: special, general, and cosmological*. Oxford University Press, Oxford
- Robertson H., 1938, *Annals of Mathematics*, 39, 101
- Schäfer G., Wex N., 1993a, *Physics Letters A*, 174, 196
- Schäfer G., Wex N., 1993b, *Physics Letters A*, 177, 461
- Schiff L., 1960, *Phys. Rev. Lett.*, 4, 215
- Silva H. O., Holgado A. M., Cárdenas-Avedaño A., Yunes N., 2021, *Phys. Rev. Lett.*, 126, 181101
- Smarr L. L., Blandford R., 1976, *ApJ*, 207, 574
- Soffel M. H., 1989, *Relativity in Astrometry, Celestial Mechanics and Geodesy*. Springer, Heidelberg
- Thorne K. S., 1986, in *Highlights of Modern Astrophysics: Concepts and Controversies*, Shapiro S. L., Teukolsky S. A., Salpeter E. E., eds., Wiley, NY, p. 103
- Thorne K. S., 1988, in *Near Zero: New Frontiers of Physics*, Fairbank J. D., Deaver Jr. B. S., Everitt C. W. F., Michelson P. F., eds., pp. 573–586
- Thorne K. S., MacDonald D. A., Price R. H., eds., 1986, *Black Holes: The Membrane Paradigm*. Yale University Press, Yale
- Wex N., 1995, *Classical and Quantum Gravity*, 12, 983
- Wex N., 1998, *MNRAS*, 298, 67